Supporting Information

Middlebrook et al. 10.1073/pnas.1110052108

SI Text

Calculation of Secondary Organic Aerosol (SOA) Mass Yield. The mass flux of SOA into the atmosphere was used to estimate the yield of SOA from the amount of oil reaching the surface. The downwind, horizontal flux through a plane perpendicular to the wind direction was calculated from the integral of the concentration of SOA over the area of the plume multiplied by the wind speed. In a well-mixed boundary layer of known height, a single aircraft transect across the plume was sufficient to determine this flux. A trigonometric correction was made if the aircraft did not fly exactly perpendicular to the wind carrying the plume. Determining the flux from aircraft data in a well-mixed boundary layer is a standard method (1–4).

On June 10, the SOA flux 40 to 50 km downwind of the spill was about 1.1×10^5 kg day^{-1} [Fig. 6; this is slightly higher than the flux reported earlier by de Gouw *et al.*, (5) using preliminary data]. From the same aircraft flights, Ryerson et al. (6) estimated that about 1.3×10^6 kg day^{-1} of oil surfaced. Therefore, the SOA particles produced downwind represented about 8% of the oil reaching the surface. A similar percentage was estimated by comparing SOA to specific compounds. For example, C_9 aromatics were about 1.7% of the leaking oil and about 60% of them reached the surface (6), so the oil reaching the surface contained about 1% C_9 aromatics. On the two farthest downwind plume passes, the SOA mass flux was 6.5 and 10 times the flux of C_9 aromatic hydrocarbons (Fig. 6). Therefore, 6.5 to 10% of the oil reaching the surface was eventually converted to SOA mass. Note, however, that the SOA formed mainly from intermediate volatility organic compounds (IVOCs) and not from only C_9 or other aromatics (5).

The absolute flux of SOA (Fig. 6) was determined from a calculation that used boundary layer height and wind speed; therefore it had a large uncertainty. On the other hand, the yield of SOA was determined from the ratio of SOA flux to fluxes of other compounds and had a lower uncertainty. Factors leading to an underestimate of the SOA yield were that the aircraft did not sample the entire width of the aerosol plume (Fig. 2) and might not have sampled far enough downwind for the SOA formation to be completed. Indeed, Fig. 6 shows that the SOA formation rate had not become zero at the farthest downwind distance. Eventual dilution of precursors slowed the growth farther downwind of the sources. A factor leading to a possible overestimate of the yield was the treatment of unresolved species in the chromatograms that underlie the percentages of species in the leaking oil and natural gas (6). A larger flux or lower percentages of specific compounds would imply a correspondingly lower aerosol mass yield. The absolute concentrations of particulate organic material were uncertain by about ±30% (7), primarily due to uncertainties in the aerosol mass spectrometer (7, 8).

To determine the total flux of aerosol mass emitted into the atmosphere per day, SOA formation from the surface oil was scaled to the June 10 observation (of 110 metric tons/day, Fig. 6) using the estimated amount of the surface oil calculated from the daily leak rate less the daily amount of oil collected reported in the Oil Budget Calculator technical document (see www.RestoreTheGulf.gov).

$$\mathrm{SOA}_t = \mathrm{SOA}_{\mathrm{June\ 10}} \times \frac{(\mathrm{Oil\ Leaking} - \mathrm{Oil\ Captured})_t}{(\mathrm{Oil\ Leaking} - \mathrm{Oil\ Captured})_{\mathrm{June\ 10}}}$$

We did not take into account the amount of oil burned, skimmed, or chemically dispersed because we do not know quantitatively how those processes affect the SOA yield. If the oil that is burned, skimmed, or chemically dispersed is old, SOA has already formed from it. However, if the oil removed is fresh, there would be less SOA formed. It is unclear how the dispersants would affect the SOA formation. The age of the oil in these processes is uncertain for all the days of the oil leak, hence, we only used a first-order correction to the amount of leaking oil with the amount that was captured by the riser insertion tube tool and top hat. The amount of soot particles from the surface burns was calculated as 3.5% of the amount reported burned (which is considered ignited here) on a daily basis in the Oil Budget Calculator technical document (see www.RestoreTheGulf.gov).

Calculation of Emission Ratios. The emission factors for NO_x, carbon monoxide (CO), and aerosol particles were determined from the slope of the correlation of each species to carbon dioxide (CO_2). Slopes were determined from orthogonal distance linear regression fits using uncertainties estimated from the scatter in each species in other portions of the flight with very stable mixing ratios. The slopes were converted into units of emissions ratios using the relationship between CO_2 and mass of fuel ignited or burned (Fig. S2 and Table S4). For the emission ratios from the surface oil burn on June 8, aerosol extinction was converted into aerosol carbon by dividing the extinction value by a mass extinction efficiency of 8 ± 2 m^2 g^{-1} for fresh soot (9–12), using a carbon mass fraction of 1 and using a molecular weight of 12 g mol^{-1}. The amount of oil burned on the surface at that time was determined using the total amount of carbon measured in the air from CO_2, CO, and aerosol carbon, 90% of the oil ignited was emitted into the air (13), and a carbon mass fraction of 0.85 for the oil (6). For in situ burning and other combustion plumes, NO_x emission factors were determined from the reactive nitrogen (NO_y) enhancements, calculated as nitrogen dioxide (NO_2).

SOA Source in the Weather Research and Forecasting/Chemistry (WRF-CHEM) Model. We included updated SOA production mechanisms in WRF-CHEM from anthropogenic and biogenic hydrocarbons based on the volatility basis set approach (14, 15), which has been used to elucidate the mechanism of SOA formation over the *DWH* oil spill by including both volatile organic compounds (VOCs) and IVOCs (5). In the 4-km resolution model, the spatial emission pattern of the IVOCs involved in SOA formation (5) was assumed Gaussian (full-width-half-max = 12 km) and centered over the *DWH* spill site. Emissions of the measured VOCs involved in traditional SOA formation as well as NO_x from the recovery and flaring operations were confined to the 4-km grid cell containing the *DWH* site. For the 20-km resolution model, all *DWH* emissions were introduced into the grid cell containing the spill site. To compare the model SOA with hourly organic carbon (OC) data on the coast, the model SOA mass was converted into OC using a factor of 0.5 (15).

The model calculations with 4-km horizontal resolution were performed for the June 10 time period to compare the model at high spatial resolution with aircraft observations. Within 3 h downwind, the modeled SOA from the IVOCs was a significant fraction of the total SOA modeled (Fig. S3). Peak values of SOA from the *DWH* model plume were about 30% higher than the peak values observed by the aircraft and the model plume width was narrower than the measurements.

1. White WH, et al. (1976) Formation and transport of secondary air pollutants: Ozone and aerosols in the St. Louis urban plume. *Science* 194:187–189.
2. Trainer M, et al. (1995) Regional ozone and urban plumes in the southeastern United States: Birmingham, a case study. *J Geophys Res* 100:18,823–18,834.
3. Ryerson TB, et al. (1998) Emissions lifetimes and ozone formation in power plant plumes. *J Geophys Res* 103:22,569–22,583.
4. Ryerson TB, et al. (2001) Observations of ozone formation in power plant plumes and implications for ozone control strategies. *Science* 292:719–723.
5. de Gouw JA, et al. (2011) Organic aerosol formation downwind from the *Deepwater Horizon* oil spill. *Science* 331:1295–1299.
6. Ryerson TB, et al. (2011) Atmospheric emissions from the *Deepwater Horizon* spill constrain air-water partitioning, hydrocarbon fate, and leak rate. *Geophys Res Lett* 38:L07803.
7. Bahreini R, et al. (2009) Organic aerosol formation in urban and industrial plumes near Houston and Dallas, Texas. *J Geophys Res* 114:D00F16.
8. Middlebrook AM, Bahreini R, Jimenez JL, Canagaratna MR (2012) Evaluation of composition-dependent collection efficiencies for the Aerodyne aerosol mass spectrometer using field data. *Aerosol Sci Technol* 46:258–271.
9. Roessler DM, Faxvog FR (1980) Optical properties of agglomerated acetylene smoke particles at 0.5145-μm and 10.6-μm wavelenghths. *J Opt Soc Am* 70:230–235.
10. Mulholland GW, Choi MY (1998) Measurement of the mass specific extinction coefficient for acetylene and ethene smoke using the large agglomerate optics facility. *Twenty-Seventh Symposium (International) on Combustion*, (The Combustion Institute, Pittsburgh), pp 1515–1522.
11. Bruce CW, Stromberg TF, Gurton KP, Mozer JB (1991) Trans-spectral absorption and scattering of electromagnetic radiation by diesel soot. *Appl Opt* 30:1537–1546.
12. Schnaiter M, et al. (2003) UV-VIS-NIR spectral optical properties of soot and soot-containing aerosols. *J Aerosol Sci* 34:1421–1444.
13. Wang Z, et al. (2003) Characteristics of spilled oils, fuels, and petroleum products: 1. Composition and properties of selected oils (US Environmental Protection Agency), EPA/600/R-03/072.
14. Donahue NM, Robinson AL, Stanier CO, Pandis SN (2006) Coupled partitioning, dilution, and chemical aging of semivolatile organics. *Environ. Sci. Technol.* 40:2635–2643.
15. Murphy BN, Pandis SN (2010) Exploring summertime organic aerosol formation in the eastern United States using a regional-scale budget approach and ambient measurements. *J Geophys Res* 115:D24216.

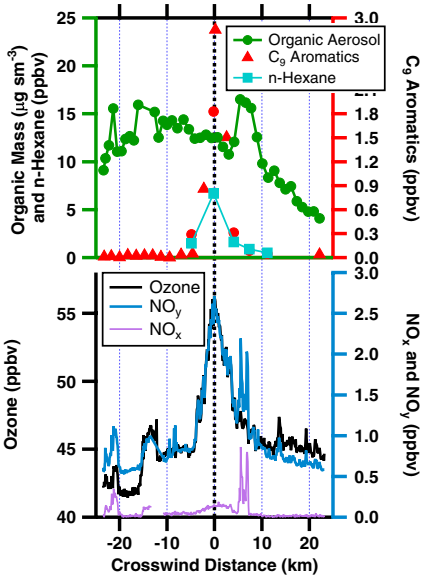

Fig. S1. Mixing ratios measured during a transect across the *DWH* pollution plume downwind from the *DWH* site. This transect was approximately 2 h later than the transect shown in Fig. 2. In the top panel, measurements of C_9 aromatics are shown from the proton-transfer-reaction mass spectrometer (PTRMS) instrument (triangles) and from the whole air sampler (circles). Combining them was necessary because the PTRMS instrument did not sample over the right side of the plume. Downwind distances from *DHW* were 47 ± 5 km except the most negative crosswind portion was 38 to 42 km downwind. Alkanes are represented by hexane in the top plot. The peaks in NO_x and NO_y to the right of the main plume were from NO_x sources close to the aircraft track that were not present in the earlier transect. ppbv, parts per billion by volume; sm, standard meter.

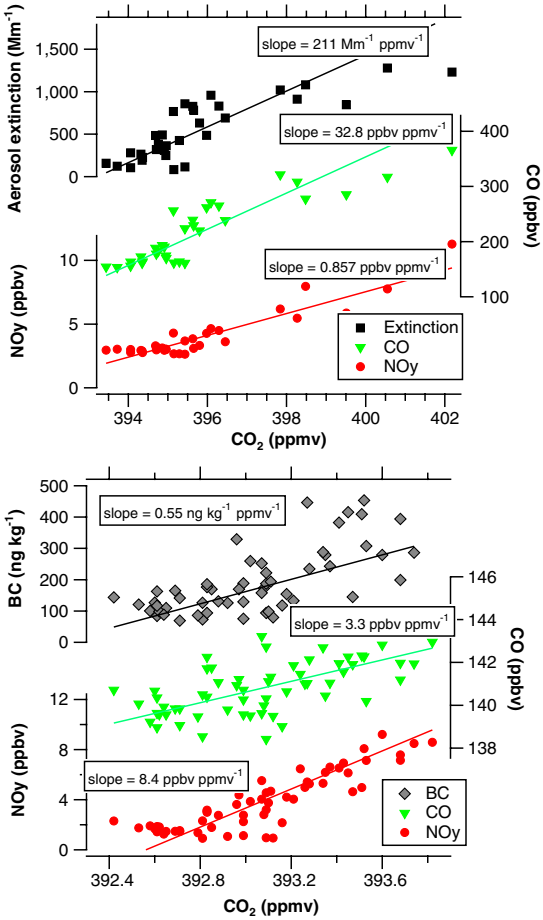

Fig. S2. Correlations to CO_2 of 1-s measurements of aerosol extinction, CO, and NO_y in the smoke plume from surface burning of oil on June 8 (*Upper*) and black carbon (BC), CO, and NO_y within plumes from containment and cleanup operations about 9 km downwind of *DWH* on June 10 (*Lower*). The linear fits were used to determine emission factors. Fits were orthogonal distance linear regression using uncertainties estimated from the scatter in each species in other portions of the flight with very stable mixing ratios. ppbv, parts per billion by volume; ppmv, parts per million by volume.

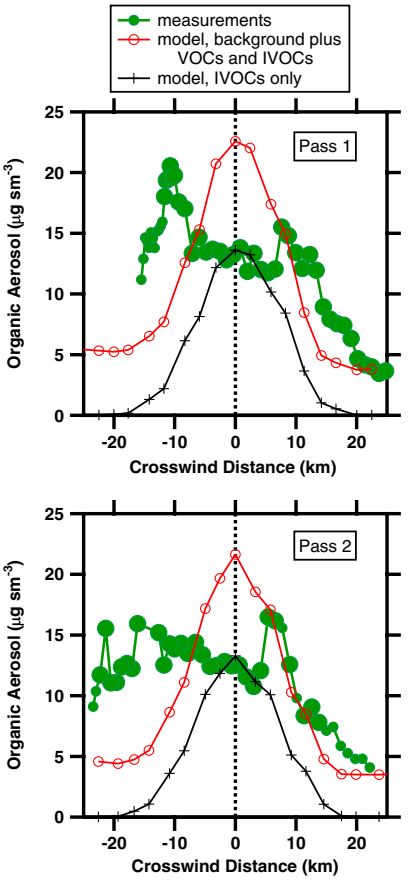

Fig. S3. The 4-km model calculated SOA and the contribution of SOA from IVOCs only compared to the measurements aboard the aircraft for the two farthest downwind passes on June 10 (Fig. 2 and Fig. S1). Downwind distances from *DWH* were 47 ± 5 km for the larger points and 26 to 42 km for the smaller points. Note that the plume from the 4-km resolution model was narrower and higher than the measurements. sm, standard meter.

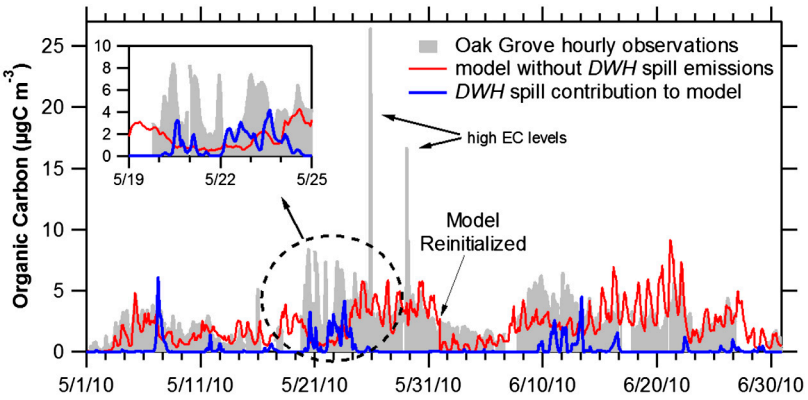

Fig. S4. The 20 km horizontal resolution WRF-CHEM model results are shown for May and June, 2010. Time series of observed particulate OC at Oak Grove, MS. Also shown are modeled concentrations without the *DWH* spill and from the spill. The effect of emissions from the spill on the measured OC is apparent during periods with onshore winds from over the spill, as depicted in the *Inset* and a few events in June.

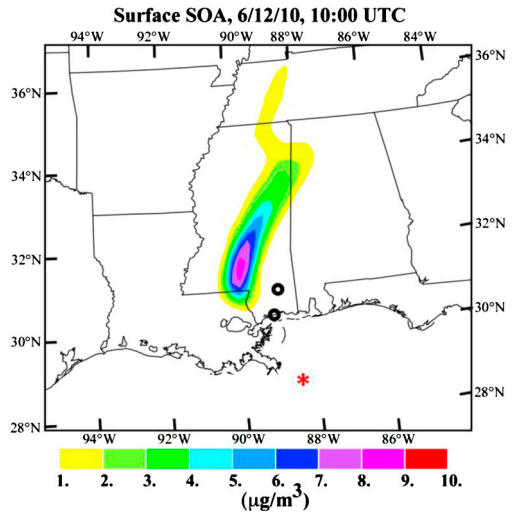

Fig. S5 Predicted surface SOA contribution from the *DWH* oil spill for the day and hour of maximum continental impact. The red asterisk shows the *DWH* spill site location. The small black circles are the locations of the Gulfport (coastal MS) and Oak Grove (inland MS) Southeastern Aerosol Research and Characterization sites. UTC, Coordinated Universal Time.

Table S1. Aerosol and gas instrumentation used in this work

Species measured	Technique or instrument name	Ref(s).
Aerosol light extinction	Cavity ring-down aerosol extinction spectroscopy	(1, 2)
Black carbon	Single-particle soot photometer	(3)
CO_2	Cavity ring-down spectroscopy	(4)
CO	Vacuum ultraviolet fluorescence	(5)
Nitric acid	Chemical ionization mass spectrometry	(6)
NO_2	Chemiluminescence	(7, 8)
Nitrogen oxide	Chemiluminescence	(7, 8)
Organic aerosol	Aerosol mass spectrometer	(9, 10)
Ozone	Chemiluminescence	(7, 8)
Particle number concentrations	Nucleation mode aerosol sizing spectrometer, ultrahigh sensitivity aerosol spectrometer, and white light optical particle counter	(11)
Peroxyacyl nitrates	Thermal dissociation-chemical ionization mass spectrometry	(12)
NO_y	Chemiluminescence	(7, 8)
VOCs	PTRMS and gas chromatography with mass spectrometry/flame ionization detector	(13–15)

Note this is not a complete list of the instrumentation installed on the airplane.

1 Langridge JM, Richardson MS, Lack D, Law D, Murphy DM (2011) Aircraft instrument for comprehensive characterization of aerosol optical properties, part I: Wavelength-dependent optical extinction and its relative humidity dependence measured using cavity ring-down spectroscopy. *Aerosol Sci Technol* 45:1305–1318.
2 Baynard T, et al. (2007) Design and application of a pulsed cavity ring-down aerosol extinction spectrometer for field measurements. *Aerosol Sci Technol* 41:447–462.
3 Schwarz JP, et al. (2006) Single-particle measurements of midlatitude black carbon and light-scattering aerosols from the boundary layer to the lower stratosphere. *J Geophys Res* 111:D16207.
4 Model G1301-m, Picarro Instruments, Santa Clara, CA.
5 Holloway JS, et al. (2000) Airborne intercomparison of vacuum ultraviolet flouorescence and tunable diode laster absroption measurements of tropospheric carbon monoxide. *J Geophys Res* 105:24251–24261.
6 Neuman JA, et al. (2009) Relationship between photochemical ozone production and NO_x oxidation in Houston, Texas. *J Geophys Res* 114:D00F08.
7 Ryerson TB, et al. (1999) Design and initial characterization of an inlet for gas-phase NO_y measurements. *J Geophys Res* 104:5483–5492.
8 Ryerson TB, Williams EJ, Fehsenfeld FC (2000) An efficient photolysis system for fast-response NO_2 measurements. *J Geophys Res* 105:26,447–26,461.
9 Canagaratna MR, et al. (2007) Chemical and microphysical characterization of ambient aerosols with the Aerodyne aerosol mass spectrometer. *Mass Spectrom Rev* 26:185–222.
10 Bahreini R, et al. (2009) Organic aerosol formation in urban and industrial plumes near Houston and Dallas, Texas. *J Geophys Res* 114:D00F16.
11 Brock CA, et al. (2008) Sources of particulate matter in the northeastern United States in summer: 2.Evolution of chemical and microphysical properties. *J Geophys Res* 113: D08302.
12 Slusher DL, Huey LG, Tanner DJ, Flocke FM, Roberts JM (2004) A thermal dissociation-chemical ionization mass spectrometry (TD-CIMS) technique for the simultaneous measurement of peroxyacyl nitrates and dinitrogen pentoxide. *J Geophys Res* 109:D19315.
13 de Gouw JA Warneke C (2007) Measurements of volatile organic compounds in the Earth's atmosphere using proton-transfer-reaction mass spectrometry. *Mass Spectrom Rev* 26:223–257.
14 Baker AK, et al. (2008) Measurements of nonmethane hydrocarbons in 28 United States cities. *Atmos Environ* 42:170–182.
15 Air Chemistry in the Gulf of Mexico Oil Spill Area, available at http://www.esrl.noaa.gov/csd/tropchem/2010gulf/GulfReport.pdf.

Table S2. Statistical summary of aircraft measurements within the MBL in the boxes illustrated in Fig. 1

		Deepwater Horizon spill region		Downwind *Deepwater Horizon* plume		Near shore		Background or upwind Gulf air	
Variable	Units	Avg	Max	Avg	Max	Avg	Max	Avg	Max
June 8									
Ozone	ppbv	57	83	45	60	54	69	30	35
Carbon monoxide	ppbv	145	152	140	163	156	168	90	97
Nitrogen dioxide	ppbv	0.1	0.5	0.1	1.3	0.1	2.1	0.1	1.6
PANs	ppbv	0.4	1.0	0.3	0.6	0.3	0.6	0.1	0.1
Acetaldehyde	ppbv	2.0	3.4	1.1	2.7	0.50	0.7	0.3	0.5
Benzene	ppbv	0.2	0.5	0.1	0.2	<0.05	0.1	<0.05	0.1
Toluene	ppbv	0.6	2.1	<0.05	0.3	<0.05	0.1	<0.05	<0.05
C8 aromatics	ppbv	1.6	6.0	<0.05	0.6	<0.05	<0.05	<0.05	<0.05
C9 aromatics	ppbv	1.9	9.2	0.1	0.8	<0.05	<0.05	<0.05	<0.05
C10 aromatics	ppbv	1.1	3.8	<0.05	0.4	<0.05	<0.05	<0.05	<0.05
C11 aromatics	ppbv	0.6	1.7	<0.05	0.2	<0.05	<0.05	<0.05	<0.05
Naphthalene	ppbv	0.3	0.5	<0.05	0.2	<0.05	<0.05	<0.05	<0.05
AMS total mass	$\mu g\,sm^{-3}$	23.0	30.8	24.0	42.4	11.7	23.5	3.3	5.1
AMS organic mass	$\mu g\,sm^{-3}$	19.0	26.2	19.5	38.2	7.1	18.2	0.3	1.2
AMS sulfate mass	$\mu g\,sm^{-3}$	2.6	3.3	3.1	5.1	3.4	6.9	2.4	3.5
Black carbon mass	$\mu g\,sm^{-3}$	0.4	1.3	0.1	0.2	0.1	0.2	0.1	0.1
Sampling transect	km	26		92		260		53	
June 10									
Ozone	ppbv	47	50	46	56	52	63	46	48
CO	ppbv	139	143	139	152	135	151	133	138
Nitrogen dioxide	ppbv	0.6	4.4	0.1	1.5	<0.05	1.0	<0.05	0.2
PANs	ppbv	0.1	0.2	0.2	0.5	0.2	0.3	0.1	0.1
Acetaldehyde	ppbv	0.5	0.9	0.6	1.5	0.4	0.7	0.3	0.4
Benzene	ppbv	0.1	1.0	<0.05	0.3	<0.05	0.1	<0.05	0.1
Toluene	ppbv	0.2	2.5	0.1	1.0	<0.05	<0.05	<0.05	<0.05
C8 aromatics	ppbv	0.4	7.3	0.2	3.1	<0.05	<0.05	<0.05	<0.05
C9 aromatics	ppbv	0.6	8.4	0.3	5.5	<0.05	<0.05	<0.05	<0.05
C10 aromatics	ppbv	0.4	2.6	0.2	3.3	<0.05	<0.05	<0.05	<0.05
C11 aromatics	ppbv	0.3	1.6	0.1	1.7	<0.05	<0.05	<0.05	<0.05
Naphthalene	ppbv	0.1	0.4	0.1	0.3	<0.05	<0.05	<0.05	<0.05
AMS total mass	$\mu g\,sm^{-3}$	8.7	13.5	14.4	25.7	7.6	14.8	6.9	8.7
AMS organic mass	$\mu g\,sm^{-3}$	4.6	8.6	10.3	20.5	3.4	11.3	2.0	2.6
AMS sulfate mass	$\mu g\,sm^{-3}$	3.2	3.9	3.0	3.9	3.1	5.8	3.7	4.9
Black carbon mass	$\mu g\,sm^{-3}$	0.2	0.7	0.1	0.3	0.1	0.2	0.1	0.2
Sampling transect	km	25		40		260		16	

Maximum values are the maximum averages over 1 km of flight path. The aerosol mass concentrations do not include nonvolatile material or particles larger than about 0.6 micrometer diameter. AMS, aerosol mass spectrometer; PANs, peroxyacyl nitrates; ppbv, parts per billion by volume; sm, standard meter.

Table S3. Statistical summary of selected hydrocarbon mixing ratios (in ppbv)

Species	Ship Avg	Ship Max	June 8 Avg	June 8 Max	June 10 Avg	June 10 Max	HGB Avg	HGB Max	GoM Avg	GoM Max
Ethane	0.42	0.66	2.8	3.0	1.2	1.4	8.4	197.0	0.39	3.93
Propane	4.2	121	6.5	12.7	0.5	2.7	6.4	347.5	0.18	4.06
n-Butane	41	1080	15.4	28.8	3.4	21.7	4.2	467.6	0.14	1.59
Isobutane	17	392	5.5	10.4	1.0	6.3	4.4	182.1	0.041	0.54
n-Pentane	48	977	15.5	25.4	5.9	36.1	2.2	183.1	0.044	0.43
Methylcyclopentane	25	333	5.1	8.8	2.2	12.9	0.36	31.4	0.002	0.019
Cyclohexane	27	316	4.6	7.9	2.0	11.3	0.32	22.6	0.001	0.014
n-Hexane	44	671	12.7	22.0	5.6	32.2	0.86	80.9	0.010	0.115
Methylcyclohexane	47	671	11.7	20.9	5.6	31.0	0.21	23.6	0.001	0.021
n-Octane	24	383	7.8	14.1	3.6	18.6	0.09	9.4	bdl	0.005
n-Decane	14	215	4.3	8.1	2.2	10.1	0.06	3.4	0.002	0.005
Benzene	0.05	0.47	0.1	0.2	0.0	0.1	0.42	11.9	0.007	0.014
Toluene	2.8	61	0.8	1.6	0.1	1.0	0.50	15.9	0.002	0.012
Sum of m- & p-xylenes	14	298	1.7	6.0	1.3	8.3	0.22	11.0	0.002	0.012
o-Xylene	2.1	53	1.1	4.0	0.3	1.9	0.09	3.9	0.001	0.005
Ethyl benzene	1.6	37	0.8	2.6	0.2	1.3	0.08	3.8	0.001	0.005
1,2,3-Trimethylbenzene	4.3	69	1.0	1.9	0.2	1.3	0.02	1.2	bdl	0.001
1,2,4-Trimethylbenzene	6.4	110	1.5	3.7	0.7	4.4	0.08	3.8	bdl	0.003
1,3,5-Trimethylbenzene	4.6	80	0.5	1.3	0.4	2.0	0.02	1.1	bdl	0.001
2-Ethyltoluene	0.89	17	0.4	0.9	0.2	1.1	0.02	1.0	bdl	0.001
Sum of 3- & 4-ethyltoluenes	6.4	119	1.3	2.9	0.6	3.3	0.08	5.7	bdl	0.003
n-Propylbenzene	0.39	7.6	0.3	0.8	0.2	1.0	0.02	0.8	bdl	bdl
Isopropylbenzene	0.24	2.8	bdl	bdl	bdl	bdl	0.02	1.1	bdl	bdl

The ship data were obtained on June 22–27, 2010 from the National Oceanic and Atmospheric Administration (NOAA) ship *Thomas Jefferson* within a 10 km radius of the *DWH* site. The June 8 and 10 data were obtained in 2010 from the closest aircraft transects. The data for the Houston and Galveston Bay (HGB) and Central Gulf of Mexico (GoM) areas were obtained from another NOAA research ship in 2006 (1). Bdl, measurements consistently below the detection limits; ppbv, parts per billion by volume.

1 Gilman JB, et al. (2009) Measurements of volatile organic compounds during the 2006 TexAQS/GoMACCS campaign: Industrial influences, regional characteristics, and diurnal dependencies of the OH reactivity. *J Geophys. Res* 114:D00F06.

Table S4. Emission factors from in situ burning of surface oil and flaring, recovery, and cleanup operations

	In situ burning of surface oil (June 8 only)		Flaring, recovery, and cleanup operations		
Species	Emission factor ($g\,kg^{-1}$ fuel burned)	Comparisons (references)	Emission factor range ($g\,kg^{-1}$ fuel burned)	Emission factor median	Comparisons (references)
NO_y (as NO_2)	2.3	0.9–1.2 (1)	1.4–37	27	flaring 1.4 (2)* oil tankers 28–79 (3)
CO	54	30 (1) 105 (4)	5–22	11	flaring 7.6 (2)* oil tankers 3.6–17 (3)
BC as carbon	39 (aerosol extinction scaled to BC) 36 (5)	73 (1) 87 g PM kg^{-1} (1) 13–150 g kg^{-1} (4) 35–80 g kg^{-1} (6) 37–94 g kg^{-1} (7)	0.07–1.3 (from BC measurement)	0.4	nonsmoking flares approximately 0 (2) tankers and tug boats 0.38–0.97 (8)
Particle no. (0.004–1 μm diameter)	3.9×10^{15} particles kg^{-1}	$(3.5–4.0) \times 10^{15}$ particles kg^{-1} (1)			

The carbon mass fraction of the fuel is assumed to be 0.85 and 90% of the ignited fuel is assumed to have burned (9, 10). Aerosol extinction was converted into aerosol carbon using a mass extinction efficiency of 8 ± 2 $m^2\,g^{-1}$ for fresh soot (11–14). Data were considered in the plume when CO_2 enhancements were greater than 2 ppmv for the in situ burn pass or 0.7 ppm for the flaring, cleanup, and recovery plumes. Note that the uncertainties for the in situ burning values are dominated by only having measurements for a single smoke plume. For flaring, recovery, and cleanup operations there were six usable transects for BC, nine for NO_y, and nine for CO. A few transects had poor signal to noise for some species or were so short that they were sensitive to time shifts between the various instruments. BC, black carbon; ppmv, parts per million by volume.

*Used a factor of 1.9e−5 to convert from British thermal units (BTUs) to kg of methane and used the measured methane mass fraction of 0.8606 in the recovered natural gas (10) to convert from kg of methane to kg of fuel.

1 Ross JL, Ferek RJ, Hobbs PV (1996) Particle and gas emissions from an in situ burn of crude oil on the ocean. *J Air Waste Manag Assoc* 46:251–259.
2 US Environmental Protection Agency (1995), Compilation of air pollutant emission factors, Volume 1: Stationary point and area sources, AP-42.
3 Williams EJ, Lerner BM, Murphy PC, Herndon SC, Zahniser MS (2009) Emissions of NO_x, SO_2, CO, and HCHO from commercial marine shipping during Texas Air Quality Study (TexAQS) 2006. *J Geophys Res* 114:D21306.
4 Evans DD, Mulholland GW, Baum HR, Walton WD, McGrattan KB (2001) In situ burning of oil spills. *J Res Natl Inst Stand Technol* 106:231–278.
5 Perring AE, et al. (2011) Characteristics of black carbon aerosol from a surface oil burn during the *Deepwater Horizon* oil spill. *Geophys Res Lett* 38:L17809.
6 Benner BA, et al. (1990) Polycyclic aromatic hydrocarbon emission from the combustion of crude oil on water. *Environ Sci Technol* 24:1418–1427.
7 Aurell J, Gullett BK (2010) Aerosat sampling of PCDD/PCDF emissions from the Gulf oil spill in situ burns. *Environ Sci Technol* 44:9431–9437.
8 Lack DA, et al. (2009) Particulate emissions from commercial shipping: Chemical, physical, and optical properties. *J Geophys Res* 114:D00F04.
9 Fingas MF, et al. (1996) Emissions from mesoscale in situ oil fires: The Mobile 1991 experiments. *Spill Sci Technol B* 3:123–137.
10 Ryerson TB, et al. (2011) Atmospheric emissions from the *Deepwater Horizon* spill constrain air-water partitioning, hydrocarbon fate, and leak rate. *Geophys Res Lett* 38:L07803.
11 Roessler DM, Faxvog FR (1980) Optical properties of agglomerated acetylene smoke particles at 0.5145-μm and 10.6-μm wavelenghths. *J Opt Soc Am A* 70:230–235.
12 Bruce CW, Stromberg TF, Gurton KP, Mozer JB (1991) Trans-spectral absorption and scattering of electromagnetic radiation by diesel soot. *Appl Opt* 30:1537–1546.
13 Mulholland GW, Choi MY (1998) Measurement of the mass specific extinction coefficient for acetylene and ethene smoke using the large agglomerate optics facility. *Twenty-Seventh Symposium (International) on Combustion*, (The Combustion Institute, Pittsburgh), pp 1515–1522.
14 Schnaiter M, et al. (2003) UV-VIS-NIR spectral optical properties of soot and soot-containing aerosols. *J Aerosol Sci* 34:1421–1444.